

IMECE2007-41604

NUMERICAL ANALYSIS OF A PLANAR WAVE PROPAGATION BASED MICROPROPULSION SYSTEM

A.F. Tabak

Faculty of Engineering and Natural Sciences
Sabanci University, Istanbul, Turkey
tabak@su.sabanciuniv.edu

S. Yeşilyurt

Faculty of Engineering and Natural Sciences
Sabanci University, Istanbul, Turkey
syesilyurt@sabanciuniv.edu

ABSTRACT

Micropropulsion mechanisms differ from macro scale counterparts owing to the domination of viscous forces in microflows. In essence, propulsion mechanisms such as cilia and flagella of single celled organisms can be deemed as nature's solution to a challenging problem, and taken as a basis for the design of an artificial micropropulsion system. In this paper we present numerical analysis of the flow due to oscillatory planar waves propagating on microstrips. The time-dependent three-dimensional flow due to moving boundaries of the strip is governed by incompressible Navier-Stokes equations in a moving coordinate system, which is modeled by means of an arbitrary Lagrangian-Eulerian formulation. The fluid medium surrounding the actuator boundaries is bounded by a channel, and neutral boundary conditions are used in the upstream and downstream. Effects of actuation parameters such as amplitude, excitation frequency, wavelength of the planar waves are demonstrated with numerical simulations that are carried out by third party software, COMSOL. Functional-dependencies with respect to the actuation parameters are obtained for the average velocity of the strip and the efficiency of the mechanism.

INTRODUCTION

Propulsion mechanisms of microswimmers can be imitated as artificial propulsion systems to operate in low Reynolds number environments. A series of theoretical work focus on natural microswimmers and their actuation principles [1-7]. It was shown that inside highly viscous fluids with low Reynolds number, a conventional time reversible swimming action can not yield desired propulsive effect due to 'scallop theorem' [1].

Microswimmers, which usually are single celled organisms like spermatozoa, employ planar or helical wave propagation via their flagellum and cilia called organelles [2,3]. Periodic traveling-wave deformations on the biopolymer tail of the microorganism are the result of the balance between the bending stresses of the structure and the total stress in the fluid [4]. Sir Taylor presented asymptotic solutions of the flow for a sinusoidal wave propagating on an infinite inextensible sheet immersed in a viscous fluid [5]. Later, Katz presented an asymptotic solution for the infinite sheet placed inside a channel [6]. Childress [7] expanded the study to extensible sheet propulsion. Our previous work verifies asymptotic results of Taylor [5] and Katz [6] by means of numerical solution of the two-dimensional time-dependent Stokes flow due to plane waves traveling on a finite-length thin membrane inside a channel [8]. Although time irreversible wave propulsion is the method utilized by natural microswimmers, efficiency of these swimmers is found to be very low due to high shear losses [9].

The micro-surgical-swimmer idea was articulated by Richard Feynman as an example to the potential upcoming micro applications [10,11]. Recently, theoretical and experimental studies were published on the propulsion of autonomous swimming robots utilizing biological mechanisms [12,13,14]. A conceptual design utilizing rotational motion to create propulsive effect for a surgical microswimmer was discussed by Edd *et al.* [12]. Furthermore, beating motion on a single filament was replicated artificially by wave propagation on a synthetic tail made by magnetic filaments attached to blood-cells and driven by alternating external magnetic fields [15]. Also macro scale experiments were carried out to demonstrate the feasibility of planar

and helical wave propagation as propulsion method [16,17].

Traveling wave propagation on an electrically driven Nafion based tail in centimeter scale proved to be viable as a propulsion system [16] at low frequencies. Similarly, three-dimensional numerical investigation of surface acoustic waves created by interdigital transducers on a thin membrane was carried out as an actuation method at large frequency despite the small amplitude of the acoustic waves [18]. Furthermore it is plausible to suggest that the wave propagation effect can also be sustained by a series of piezoelectric material replaced in series and driven out-of-phase via shear mode piezo strips [19,20,21].

Vertical traveling-wave motion of the fully submerged elastic rod tail causes dynamic high and low pressure regions to shift positions resulting in net fluid flow. As the deformation shifts position accordingly with the propagation of traveling waves, high and low pressure regions in the vicinity of the tail demonstrate consequential shifts which result in two-dimensional thrust effect. This resultant shifts cause a combinational force interactions between swimmer body and surrounding fluid which leads to translations along both x -axis and y -axis and rotation around z -axis.

We present numerical simulations of 3D time-dependent motion of a conceptual swimming micro-robot, inside a liquid filled channel due to the propagation of sine-wave deformations on a long conical tail attached to a capsule. The motion of the swimmer is governed by rigid-body equation of motion which incorporates the forces and moments from the motion of the fluid governed by incompressible Navier-Stokes equations subject to continuity in a time-varying domain that has moving boundaries due to the motion of the tail as well as the motion of the robot. Mesh displacement due to moving boundaries of the tail is modeled using arbitrary Lagrangian-Eulerian formulation [22,23] incorporating the Winslow method [24]. Effects of the amplitude, frequency, wave length and homogeneity of traveling waves on the speed, hydraulic power and efficiency are demonstrated.

NOMENCLATURE

Symbol	Description
Latin Letters	
A	Area
B	Wave amplitude
C	Wave limiting constant

METHODOLOGY

Three-dimensional motion of the swimmer has four distinctive elements: First is the traveling-plane wave deformation of the tail, which transfers the

H	Channel height
I	Identity matrix
J	Mass moment of inertia
L	Channel length
M	Mass of the swimmer
M	Moment on swimmer
P	Liquid pressure
Q	Flow rate
\bar{S}	Swimmer surface
U	Fluid velocity vector
W	Width
f	Excitation frequency [Hz]
k	Wave number
ℓ	Tail length
n	Surface normal vector
r	Distance from center of mass
t	Spatial time
t	Surface tangent vector
u	Mesh velocity vector
u,v,w	velocity components
x,y,z	Spatial coordinates

Functions and Groups

B	Amplitude expression
min	Minimum function
Re	Reynolds Number

Greek Letters

θ	Rotation angle to center of mass
Π	Mechanical Power exerted on fluid
Σ	Mono directional full stress tensor
Ω	Domain occupied by fluid inside
α	Angle between r and x -axis
η	Percentage mechanical efficiency
λ	Wave length
μ	Dynamic viscosity of liquid
ρ	Liquid density
ω	Angular frequency

Subscripts and Superscripts

A_{av}	Area-averaged
av	Time-averaged
ch	Channel parameter
com	Center of mass
f	Tail parameter
in,out	Inwards/outwards direction
m	Mesh parameter
o	Maximum possible value
o	Flow development time
sim	Simulation Parameter
sh	Wave shape parameter
T	Transpose

energy from the structure to the flow; second and third elements are x and y -translations of the swimmer and lastly the z -rotation of the swimmer around its center of mass.

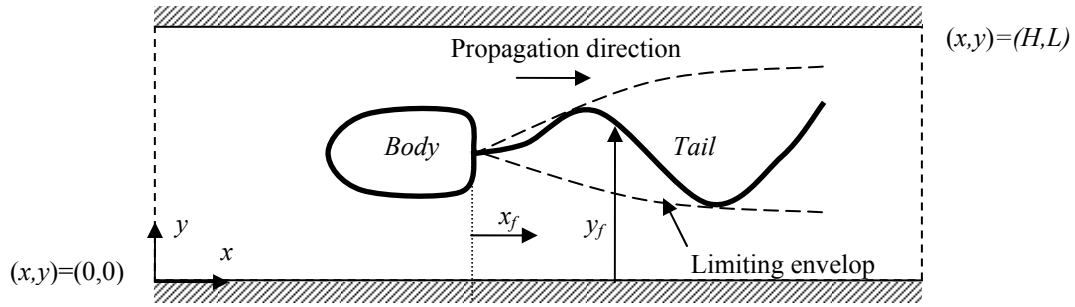


Figure 1: Plane-wave deformations traveling in the x -direction on the tail attached to the head of the swimming robot; side-view in the z -direction on the xy -symmetry plane.

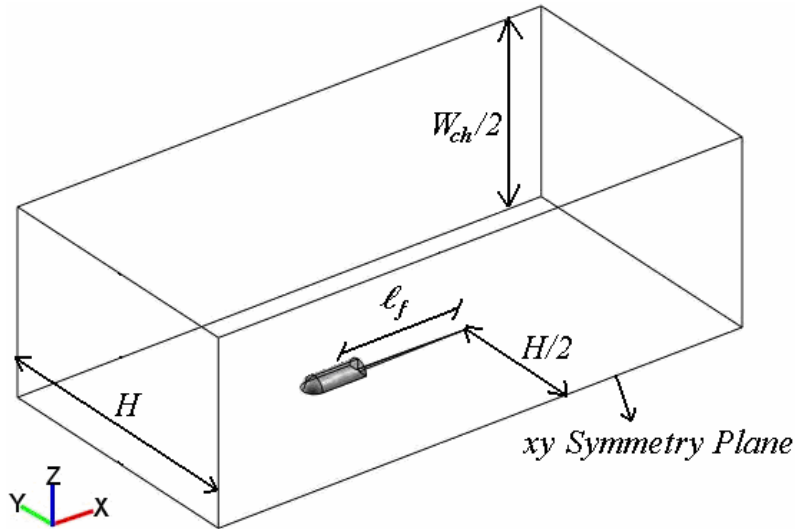


Figure 2: 3D view of conceptual swimming microrobot and the channel; cut into two symmetric pieces with respect to xy -symmetry plane.

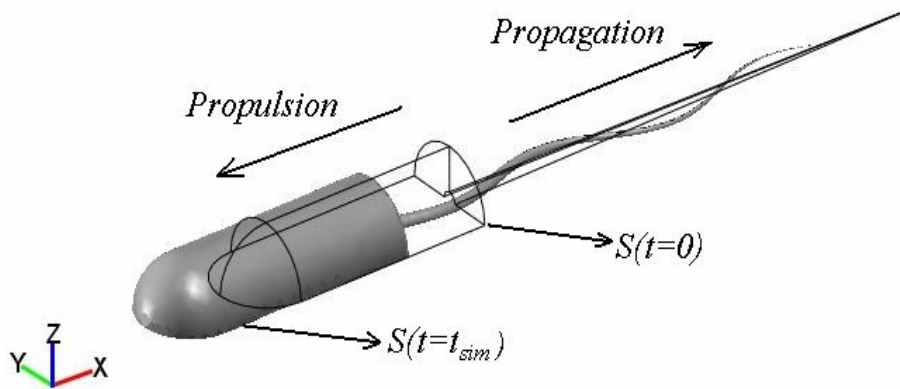


Figure 3: 3D view of conceptual swimming microrobot; net propulsion and wave propagation wakes place on opposite sides.

Motion of the tail in the xy -plane is perpendicular to the wave propagation in the x -direction as shown in Fig. 1, and given by a sinusoidal wave-form as a function of time, t , x -position on the tail, x_f , exci-

tation frequency, $\omega=2\pi f$, wave number, $k=2\pi/\lambda$ and the amplitude function B , i.e.

$$y_f(x_f, t) = B \sin(\omega t - kx_f), \quad x_f > 0 \quad (1)$$

In Eq. (1), $B=B(x_f,t)$ forms an envelop function for deformations in the y -direction resulting in one end being free and the other end attached to the body at all times. Furthermore, to ensure zero initial conditions, an initial ramp of the amplitude of deformations is defined and restricted to the first full period:

$$B(x_f,t) = B_0 \left\{ 1 - \exp \left[-C_{sh} (x_f - x_{com}) \right] \right\} \min(t, 1/f) \quad (2)$$

where C_{sh} is the shape constant for limiting amplitude envelope, x_{com} is the x -coordinate of the center of mass which is on the rigid joint between tail and body.

Translation in the x -direction is due to the thrust force exerted by the y direction motion of the tail, and calculated from the equation of motion:

$$\ddot{x}_S = \frac{1}{M} \int_{S(t)} \Sigma_x dS \quad (3)$$

where, M is the mass of the neutrally buoyant swimmer and Σ_x is the x -component of the full stress tensor, which is given by [25]:

$$\Sigma_x = \begin{bmatrix} \left(2\mu \frac{\partial u}{\partial x} - P \right) \\ \mu \left(\frac{\partial u}{\partial y} + \frac{\partial v}{\partial x} \right) \\ \mu \left(\frac{\partial u}{\partial z} + \frac{\partial w}{\partial x} \right) \end{bmatrix} \cdot \mathbf{n} \quad (4)$$

Translation in the y -direction is calculated in the same manner as in Eq. (3) but with the y component of the full stress tensor as follows

$$\ddot{y}_S = \frac{1}{M} \int_{S(t)} \Sigma_y dS \quad (5)$$

where

$$\Sigma_y = \begin{bmatrix} \mu \left(\frac{\partial u}{\partial y} + \frac{\partial v}{\partial x} \right) \\ \left(2\mu \frac{\partial v}{\partial y} - P \right) \\ \mu \left(\frac{\partial v}{\partial z} + \frac{\partial w}{\partial y} \right) \end{bmatrix} \cdot \mathbf{n} \quad (6)$$

Rotation around the center of mass, which is at the rigid connection between the body and the tail of the swimmer, in the z -direction is obtained from

$$\ddot{\theta} = \frac{1}{J} \int_{S(t)} \mathbf{M}_z dS \quad (7)$$

where, J is the z -moment of inertia, and \mathbf{M}_z is the z -moment and given by

$$\mathbf{M}_z = \int_{S(t)} (\Sigma_x \sin \alpha + \Sigma_y \cos \alpha) r_{com} dS. \quad (8)$$

In Eq. (8) r_{com} is the distance of a point on the swimmer's surface from the center of mass of the swimmer, and α is the angle between the position vector of a point on the swimmer surface and the x -axis.

In order to model the flow around the swimmer, incompressible Navier-Stokes equations are used in the time-dependent domain $\Omega(t)$:

$$\rho \left(\frac{\partial \mathbf{U}}{\partial t} + (\mathbf{U} - \mathbf{u}_m) \cdot \nabla \mathbf{U} \right) = -\nabla P + \mu \nabla^2 \mathbf{U} \quad (11)$$

$$\nabla \cdot \mathbf{U} = 0 \quad (12)$$

where $\mathbf{U}=[u,v,w]^T$ is the velocity vector, P is pressure, ρ is density, and μ is the viscosity of the fluid. The time-dependent domain, $\Omega(t)$ deforms according to the moving boundaries of the swimmer and its tail. The \mathbf{u}_m in Eq. (11) is the deformation velocity of the mesh used in the finite-element solution of Navier-Stokes equations. Since the mesh deforms only on the swimmer boundaries and remains fixed at the channel walls, inlet and outlet, a gradual deformation of the mesh is specified between the moving swimmer and the fixed boundaries.

Channel walls are subjected to no-slip boundary conditions at all times,

$$\begin{bmatrix} u(x,0,z,t) \\ v(x,0,z,t) \\ w(x,0,z,t) \end{bmatrix} = \begin{bmatrix} u(x,H,z,t) \\ v(x,H,z,t) \\ w(x,H,z,t) \end{bmatrix} = \begin{bmatrix} 0 \\ 0 \\ 0 \end{bmatrix} \quad (13)$$

$$\begin{bmatrix} u(x,y,0,t) \\ v(x,y,0,t) \\ w(x,y,0,t) \end{bmatrix} = \begin{bmatrix} u(x,y,W_{ch},t) \\ v(x,y,W_{ch},t) \\ w(x,y,W_{ch},t) \end{bmatrix} = \begin{bmatrix} 0 \\ 0 \\ 0 \end{bmatrix}$$

where H is the channel height and W_{ch} is the channel width. Tail does not move in z -direction as its motion is limited to the xy -plane at $z=0$ given by Eq. (1)

$$w(x_f, y_f, z_f, t) = 0 \quad (14)$$

In Eq. (14), x_f , y_f and z_f constitute the time-dependent position vector on the tail; y_f is given by Eq. (1). Y -velocity due to waving action on the tail is given by the time derivative of the displacement in Eq. (1) and other velocity components can be found like wise as in Eq. (16).

$$v_f(x_f, t) = \frac{dy_f(x_f, t)}{dt} \quad (15)$$

Hence the velocity of a point on the surface of the swimmer is obtained by combining the time derivative of Eq. (1), and integrals of (3), (5) and (7).

$$\mathbf{U}_S = \begin{bmatrix} \frac{dx_S}{dt} - r_{com} \frac{d\theta}{dt} \cos(\alpha) \\ \frac{dy_f}{dt} + \frac{dy_S}{dt} + r_{com} \frac{d\theta}{dt} \sin(\alpha) \\ 0 \end{bmatrix}_{S(t)} \quad (16)$$

Inlet and outlet surfaces are specified as neutral [24] in all simulations:

$$[-P\mathbf{I} + \boldsymbol{\sigma}] \cdot \mathbf{n} \Big|_{x=0,y,z,t} = 0 \quad (17)$$

$$[-P\mathbf{I} + \boldsymbol{\sigma}] \cdot \mathbf{n} \Big|_{x=L,y,z,t} = 0 \quad (18)$$

and xy -symmetry plane is designated as slip/symmetry [26] to cancel the tangential forces and the normal velocity on the designated boundary as in Eq. (19) and (20).

$$[-P\mathbf{I} + \boldsymbol{\sigma}] \cdot \mathbf{t} \Big|_{x,y,z,W_{ch}/2,t} = 0 \quad (19)$$

$$\mathbf{U} \cdot \mathbf{n} = 0 \quad (20)$$

where \mathbf{t} is the tangential vector of the designated boundary.

For the flow at rest, all velocity components are specified as zero to guarantee stationary initial conditions.

$$u(x, y, z, 0) = v(x, y, z, 0) = w(x, y, z, 0) = 0 \quad (21)$$

Displacement of the deforming mesh is calculated from the prescribed displacement given by Eq. (1), (3), (5) and (7) by a rubber mesh function, which limits the deformation to the vicinity of the swimmer:

$$\Delta \mathbf{x}_m = \begin{bmatrix} x_S + r_{com} \theta_x \\ y_f + y_S + r_{com} \theta_y \\ 0 \end{bmatrix} \beta(x, y, z) \quad (22)$$

where $\beta(x, y, z)$ is the rubber mesh function [22]. The mesh displacement velocity, \mathbf{u}_m , in Navier-Stokes equation is found directly from the prescribed mesh deformation:

$$\mathbf{u}_m = \frac{d\Delta \mathbf{x}_m}{dt} \quad (23)$$

Once \mathbf{u}_m is obtained from Eq. (23), finite-element representation of Navier-Stokes and continuity equations, are solved subject to boundary condi-

tions Eq. (13)-(22) by commercial finite element code, COMSOL, incorporating Intel's MKL that invokes the parallel, PARDISO solver in COMSOL [26,27].

Time-averaged velocity components of the swimming microrobot are also found by integrating Eq. (16) and averaging it over simulation time. Tangential and rotational components of the surface velocity vector vanish in time averaging and can be neglected as can be observed in Fig. 4 and Fig. 5, therefore net propulsion occurs on the opposite direction of wave propagation as depicted in Fig. 3. Swimmer's average velocity in the x -direction is given by;

$$u_{av} = \frac{f}{2} \int_{t_0}^{t_0+2/f} \frac{dx_S}{dt} dt \quad (24)$$

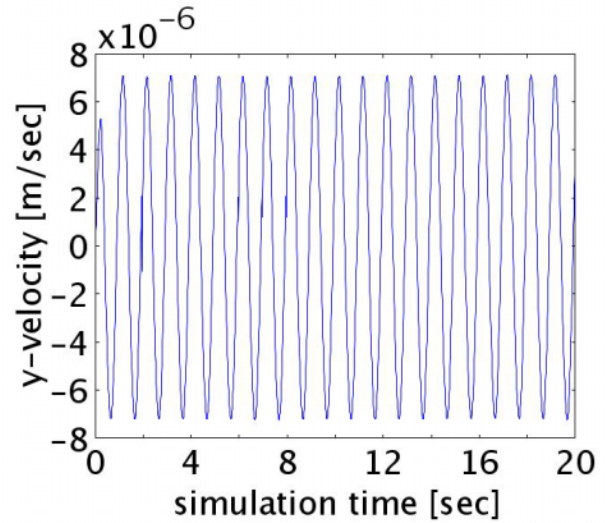


Figure 4: Instantaneous y -velocity of the swimmer.

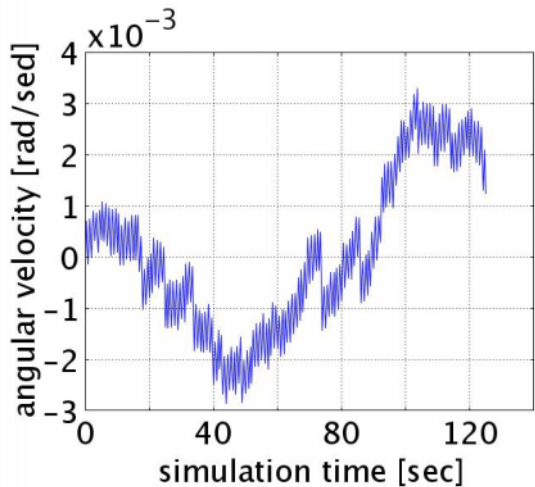


Figure 5: Instantaneous angular velocity of the swimmer.

Instantaneous rate of work done on the fluid by the deforming tail is the area integration of the product of the total y -stress and the local y -velocity, i.e.

$$\Pi(t) = \int_{A_f} \Sigma_y v_f dA_f \quad (25)$$

where A_f is the tail's surface area. Similarly to Eq. (24), time-averaged rate of work done by the tail, i.e. the hydraulic power is calculated from:

$$\Pi_{av} = \frac{f}{2} \int_{t_0}^{t_0+2/f} \Pi(t) dt \quad (26)$$

The force against average motion of the swimmer is given by

$$F_{x-av} = \frac{f}{2} \int_{t_0}^{t_0+2/f} \int_{S(t)} \Sigma_x dS dt \quad (26)$$

Finally, the efficiency of the swimmer is calculated from the ratio of the rate of work done on the fluid due to average motion of the swimmer and the rate of work done on the fluid due to motion of the tail as described by Froude efficiency formulation [28]:

$$\eta = \frac{F_{x-av} u_{av}}{\Pi_{av}} \quad (27)$$

RESULTS

Reference dimensions and properties of the swimmer are provided in Table 1 for numerical results that are presented here. For each simulation, about 33000 linear equations are solved for at least 3 time units that correspond to 3 full cycles and at least 300 time steps after simulation outputs converge to the steady-periodic state within the first cycle. Each simulation takes between 2 to 3 hours on a double dual-core 3.7 GHz 64-bit Xeon workstation with 16GB of RAM running on SUSE Linux 10.0 operating system.

Time-averaged quantities are obtained from integration over the last two cycles. Unless otherwise noted, the base case used in the simulations corresponds to $\lambda = \ell_f / 2$, $B_o = 0.073\lambda$, $f = 1$ Hz, and $C_{sh} = 6$.

Figure 6 and 7 illustrate the flow field on the symmetry plane where large circulations take place around the tip of the tail and in the downstream. Figure 7 reveals that the swimmer pushes the fluid in the propulsion direction upstream, and cause circulations behind the tail.

Figure 8 demonstrates the relationship between the amplitude and the average x -velocity of the microswimmer for all the variables fixed at the base case except the amplitude. As amplitude increases, the x -velocity increases quadratically with the change in amplitude. Figure 9 illustrates the effect of amplitude on hydraulic power which clearly shows that hydraulic power changes proportionally with the square of the change in amplitude. These results are in agreement with the asymptotical predictions stated by Taylor and Katz [5,6]. Figure 10, shows how swimmer's hydraulic efficiency behaves with respect to amplitude. It can be observed that efficiency increases very rapidly for small amplitudes but starts to plateau before reaching to 1%.

Name, symbol	Values/dimensions
W_{ch}	4×10^{-3} [m]
Channel Height, H	3×10^{-3} [m]
Channel Length, L	6×10^{-3} [m]
Tail Length, ℓ_f	1.25×10^{-3} [m]
Head Length, L_h	6.25×10^{-4} [m]
Head Radius, r_h	1.25×10^{-4} [m]
Tail width, W_f	2×10^{-5} [m]
Swimmer Mass Moment of Inertia, J	7.073456×10^{-12} [kg.m ²]
Mass of the Swimmer, M	1.713071×10^{-8} [kg]
Dynamic Viscosity of water, μ	1.12×10^{-3} [Pa.s]
Density of water, ρ	999 [kg/m ³]

Table 1: Simulation Constants

Figure 11 demonstrates the relationship between the frequency and the average x -velocity of the microswimmer for all the variables fixed at the base case except the frequency. As frequency increases, the average x -velocity increases linearly with the frequency.

Figure 12 illustrates the effect of the frequency on the power, and clearly shows that power increases proportionally with the square of the frequency.

Figure 13, efficiency of the swimmer is plotted against the frequency. The frequency of the traveling-waves does not affect the efficiency of the swimmer.

Results shown in Fig. 8 to Fig. 12 agree well with the asymptotical predictions stated by Taylor and Katz [5,6].

Figure 14 demonstrates the relationship between the wave length and the average x -velocity of the microswimmer for all variables fixed at the base case except the wave length. As wave length increases average x -velocity increases linearly with the wave length agreeing well with the asymptotic calculations of Katz [6].

Figure 15 illustrates the effect of wavelength on the power showing that as wavelength increases the power increases with $3/2^{\text{nd}}$ power of the wavelength.

Figure 16, shows the effect of the wavelength on the swimmer's hydraulic efficiency, which is not as significant as the effect of the amplitude (Fig. 10). This behavior is closer to the frequency effect (Fig. 13).

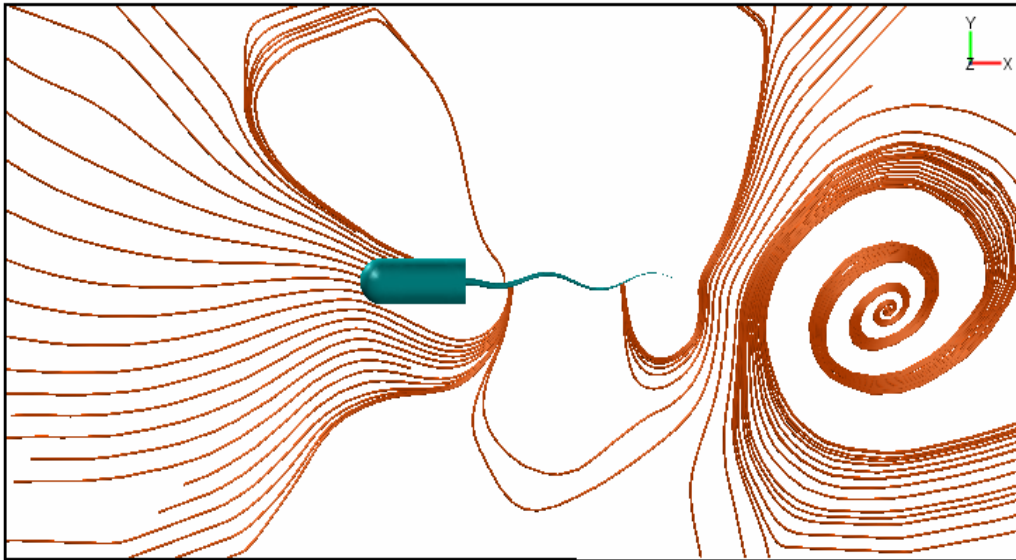


Figure 6: Swimmer microrobot with planar waves propagating on its tail. Circulations appear due to shear stresses created by the motion of the tail.

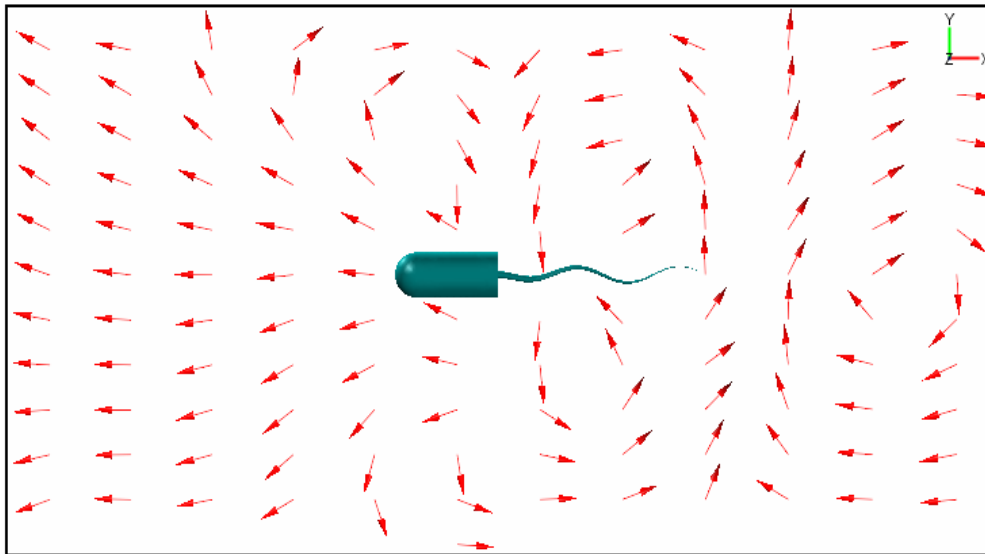


Figure 7: Normalized arrow plot demonstrating the flow field on the symmetry plane.

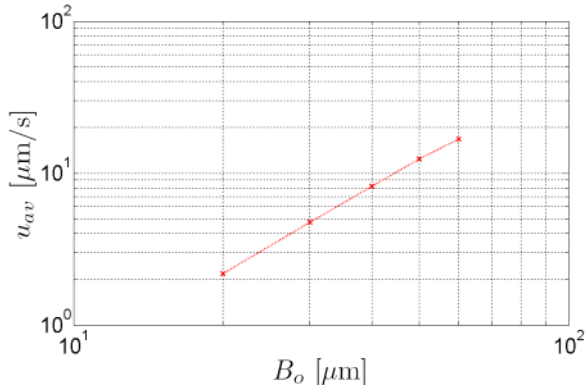


Figure 8: Wave amplitude vs. time averaged propulsion velocity for $\lambda = 625 \mu\text{m}$, $f = 1 \text{ Hz}$ and $C_{sh} = 6$.

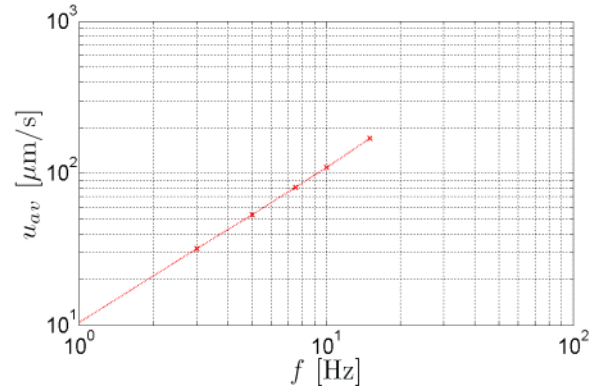


Figure 11: Driving frequency vs. time averaged propulsion velocity for $\lambda = 625 \mu\text{m}$, $B_o = 45.625 \mu\text{m}$ and $C_{sh} = 6$.

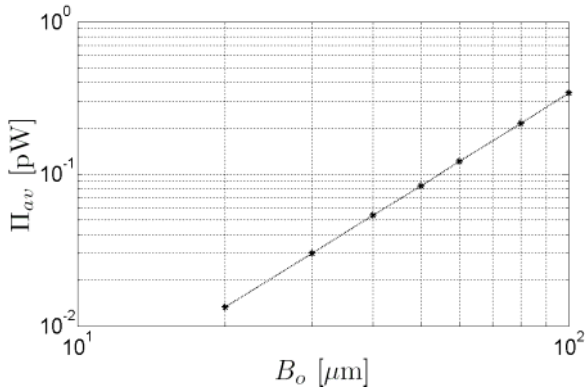


Figure 9: Wave amplitude vs. time averaged hydraulic power for $\lambda = 625 \mu\text{m}$, $f = 1 \text{ Hz}$ and $C_{sh} = 6$.

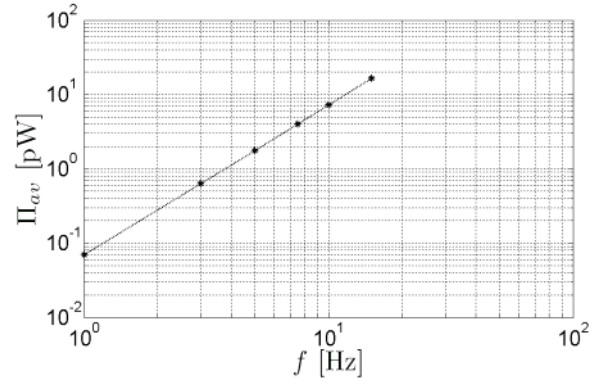


Figure 12: Driving frequency vs. time averaged hydraulic power for $\lambda = 625 \mu\text{m}$, $B_o = 45.625 \mu\text{m}$ and $C_{sh} = 6$.

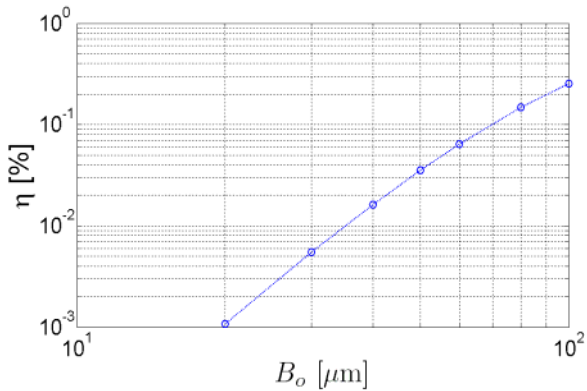


Figure 10: Wave amplitude vs. swimmer's hydraulic efficiency for $\lambda = 625 \mu\text{m}$, $f = 1 \text{ Hz}$ and $C_{sh} = 6$.

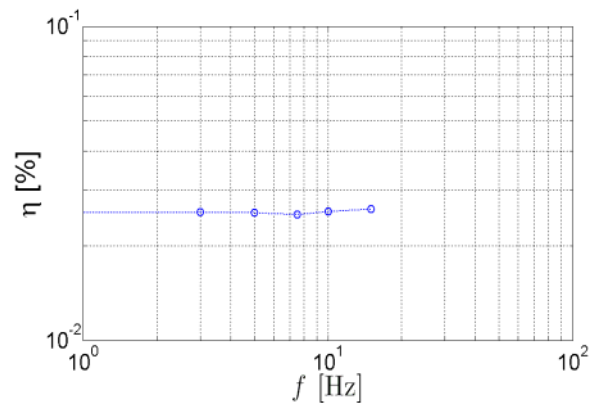


Figure 13: Driving frequency vs. swimmer's hydraulic efficiency for $\lambda = 625 \mu\text{m}$, $B_o = 45.625 \mu\text{m}$ and $C_{sh} = 6$.

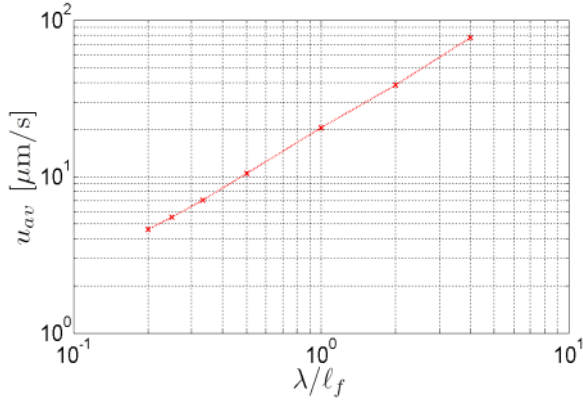


Figure 14: Ratio of wave length to tail length vs. time averaged propulsion velocity for $B_o = 45.625 \mu\text{m}$, $f = 1 \text{ Hz}$ and $C_{sh} = 6$.

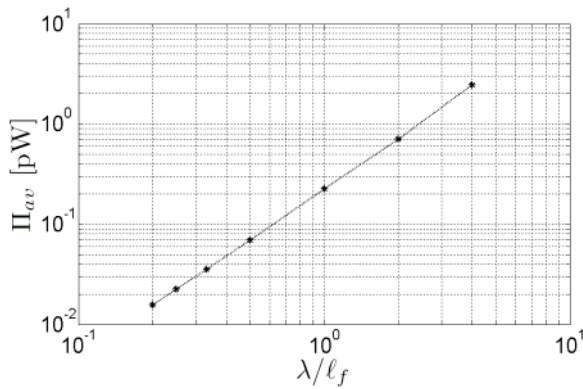


Figure 15: Ratio of wavelength to tail length vs. time averaged hydraulic power for $B_o = 45.625 \mu\text{m}$, $f = 1 \text{ Hz}$ and $C_{sh} = 6$.

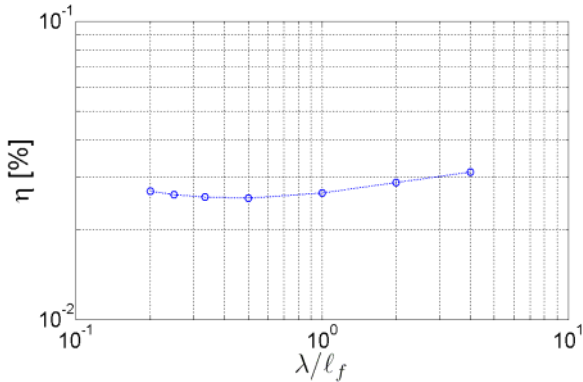


Figure 16: Ratio of wave length to tail length vs. swimmer's hydraulic efficiency for $B_o = 45.625 \mu\text{m}$, $f = 1 \text{ Hz}$ and $C_{sh} = 6$.

CONCLUSION

The effects of operating conditions, such as the wave amplitude, wavelength and excitation frequency on the propulsion performance of a microswimming

robot are demonstrated by means of three-dimensional time-dependent simulations. In simulations time-dependent three-dimensional incompressible Navier-Stokes equations subject to continuity are solved in a moving coordinate system using the arbitrary Lagrangian Eulerian method, which utilizes the Winslow smoothing.

Net x -translation, or in other words the x -thrust is modeled in accordance with the net force exerted on the swimmer surface along x -direction. Efficiency computations are based on Froude efficiency definition.

Numerical results show that y -translation and z -rotation results in zero net motion in time. Speed of the swimmer and the rate of work done on the fluid by traveling-wave deformation of the tail vary quadratically with the amplitude of the wave. Furthermore, the efficiency of the swimmer increases with the wave amplitude faster than a quadratic rate. However the effect tends to level off slightly at higher amplitudes.

Frequency has a linear effect on propulsion speed but a quadratic effect on hydraulic power; efficiency remains unaffected with the varying frequency. These results are in agreement with the earlier published asymptotical results [5,6] and our previous work on micropumps that incorporate traveling-plane wave actuators [8,29].

Wavelength has a linear effect on propulsion speed and quadratic effect on the hydraulic power verifying the asymptotic results by Katz [6]. The efficiency of the swimmer does not change with the wavelength.

ACKNOWLEDGMENTS

We kindly acknowledge the partial support for this work from the Sabanci University Internal Grant Program (contract number IACF06-00418).

REFERENCES

- [1] Purcell, E.M., 1977, "Life at Low Reynolds Number," *American Journal of Physics*, 45(1), pp. 3-11.
- [2] Brennen, C., Winet, H., 1977, "Fluid Mechanics of Propulsion by Cilia and Flagella," *Ann. Rev. Fluid Mech.*, 9, pp. 339-98.
- [3] Gray, J., Hancock, G.J., 1955, "Propulsion of Sea-Urchin Spermatozoa," *J. Exp. Biol.*, 32, pp. 802-814.
- [4] Lowe, C.P., 2003, "Dynamics of Filaments: Modeling the Dynamics of Driven Microfilaments," *Phil. Trans. R. Soc. Lond.*, B(358), pp. 1543-1550.
- [5] Sir Taylor, G., 1951, "Analysis of the Swimming of Microscopic Organisms," *Proc. Roy. Soc.*, A(209), pp. 447-61.

- [6] Katz, D.F., 1974, "On the Propulsion of Microorganisms Near Solid Boundaries," *J. Fluid Mech.*, 64(1), pp. 33-49.
- [7] Childress, S., 1981, *Mechanics of Swimming and Flying*, Cambridge Studies in Mathematical Biology, Cambridge University Press, New York, Chap. 3.
- [8] Tabak, A.F., Yesilyurt, S., 2007, "Numerical Analysis of the 3D Flow Induced by Propagation of Plane-Wave Deformations on Thin Membranes inside Microchannels," *Proceedings of the Fifth International Conference on Nanochannels, Microchannels and Minichannels*, Puebla, Mexico.
- [9] Sir Lighthill, J., 1975, *Mathematical Biofluidynamics*, Society for Industrial and Applied Mathematics, USA, Chap. 3&4.
- [10] Feynman, R.P., 1992, "There's Plenty of Room at the Bottom," *Journal of Microelectromechanical Systems*, 1(1), pp. 60-66.
- [11] Feynman, R.P., 1993, "Infinitesimal Machinery," *Journal of Microelectromechanical Systems*, 2(1), pp. 4-14.
- [12] Edd, J., Payen, S., Rubinsky, B., Stoller, M.L., Sitti, M., 2003, "Biomimetic Propulsion for a Swimming Surgical Micro-Robot," *IEEE/RSJ Intelligent Robotics and Systems Conference*, Las Vegas, USA.]
- [13] Becker, L.E., Koehler, S.A., Stone, H.A., 2003, "On Self-Propulsion of Micro-Machines at Low Reynolds Number: Purcell's Three Link Swimmer," *J. Fluid Mech.*, 490, pp.15-35.
- [14] Wiggins, C.H., Goldstein, R.E., 1998, "Flexive and Propulsive Dynamics of Elastica at Low Reynolds Number," 80(17), pp. 3879-3882.
- [15] Dreyfus, R., Baudry, J., Roper, M.L., Fermigier, M., Stoner, H.A., Bibette, J., 2005, "Microscopic Artificial Swimmers," *Nature*, 437, pp. 862-865.
- [16] Kim, B., Kim, D.-H., Jung, J., Park, J.-O., 2005, "A Biomimetic Undulatory Tadpole Robot Using Ionic Polymer-Metal Composite Actuators," *Smart Mater. Struct.*, 14, pp. 1579-1585.
- [17] Behkam, B., Sitti, M., 2006, "Design Methodology for Biomimetic Propulsion of Miniature Swimming Robots," *Journal of Dynamic Systems, Measurement, and Control*, 128, pp. 36-43.
- [18] Nguyen, N.T., White, R.M., 1999, "Design and Optimization of an Ultrasonic Flexural Plate Wave Micropump Using Numerical Simulation," *Sensors and Actuators*, 77, pp. 229-236.
- [19] Piefort, V., Henriouille, K., 2000, "Modelling of Smart Structures with Colocated Piezoelectric Actuator/sensor Pairs: Influence of the In-plane Components," *Identification, Control and Optimization of Engineering Structures*, Civil-Comp Press, Edinburgh UK.
- [20] Piefort, V., 2001, "Finite Element Modelling of Piezoelectric Active Structures. PhD Thesis submitted to Faculty of Applied Sciences," Université Libre De Bruxelles.
- [21] Hofer, M., Lerch, R., 2002, "Finite Element Calculation of Wave Propagation and Excitation in Periodic Piezoelectric Systems," Mang, H.A., Rammerstorfer, F.G., Eds., *Fifth World Congress on Computational Mechanics*, Vienna, Austria.
- [22] Tabak, A.F., 2007, "Simulation Based Experiments of Traveling-Plane-Wave-Actuator Micropumps and Microswimmers," MS Thesis submitted to Faculty of Engineering and Natural Sciences, Sabanci University.
- [23] Duarte, F., Gormaz, R., Natesan, S., 2004, "Arbitrary Lagrangian-Eulerian Method for Navier-Stokes Equations with Moving Boundaries," *Comput. Methods Appl. Mech. Engrg.*, 193, pp. 4819-4836.
- [24] Winslow, A., 1967, "Numerical Solution of the Quasilinear Poisson Equations in a Nonuniform Triangle Mesh," *J. Comp. Phys.*, 2, pp. 149-172.
- [25] Landau, L.D., Lifshitz, E.M., 2005, *Fluid Mechanics* 2nd ed., *Course of Theoretical Physics v.6*, Elsevier Butterworth-Heinemann, Oxford, Chap. 2.
- [26] COMSOL AB, 2005, *Comsol Multiphysics Modelling Guide*.
- [27] Schenk, O., Gärtner, K., 2004, "Solving Unsymmetric Sparse Systems of Linear Equations with PARDISO," *Future Generation Computer Systems*, 20(3), pp. 475-487.
- [28] Sfakiotakis, M., Lane, D.M., Davies, J.B.C., 1999, "Review of Fish Swimming Modes for Aquatic Locomotion," *IEEE Journal of Oceanic Engineering*, 24(2), pp. 237-252.
- [29] Tabak, A.F. and Yesilyurt, S., "Simulation-based analysis of flow due to traveling-plane-wave deformations on elastic thin-film actuators in micropumps", *Microfluid Nanofluid*, DOI 10.1007/s10404-007-0207-y